AIMS Materials Science, 3(1): 35-50.
DOI: 10.3934/matersci.2016.1.35
Received: 20 August 2015
Accepted: 24 December 2015
Published: 29 December 2015

http://www.aimspress.com/journal/Materials

Research article

Electrical and optical properties of hybrid polymer solar cells incorporating Au and CuO nanoparticles

Aruna P. Wanninayake, Shengyi Li, Benjamin C. Church, Nidal Abu-Zahra *

Materials Science and Engineering Department, University of Wisconsin-Milwaukee, 3200 North Cramer Street, Milwaukee, WI 53201, USA

*** Correspondence:** Email: nidal@uwm.edu; Tel: 414-229-2668.

Abstract: In this study, to enhance the power conversion efficiency (PCE) of the polymer solar cells (PSCs), Gold (Au) and Copper oxide nanoparticles (CuO-NPs) are incorporated into the PEDOT:PSS and P3HT/PCBM active layers respectively. PSCs with a constant CuO-NP content were fabricated with varying amounts of Au NPs. Addition of Au NPs increased the power conversion efficiency by up to 18% compared to a reference cell without Au-NPs. The short circuit current(J_{sc}) of the cells containing 0.06 mg of Au NPs was measured at 7.491 mA/cm^2 compared to 6.484 mA/cm^2 in the reference cells with 0.6 mg of CuO nanoparticles; meanwhile, the external quantum efficiency(EQE) increased from 53% to 61%, showing an enhancement of 15.1%. Au-NPs improved the charge collection at the anode, which results in higher short circuit current and fill factor. However, the strong near field surrounding Au-NPs due to localized surface plasmonic resonance (LSPR) effect is not distributed into the active layer. Instead, it is spread horizontally through the PEDOT:PSS layer, thus minimizing the light absorption in the active layer.

Keywords: Au nanoparticles; CuO nanoparticles; plasmonic effect; UV-visible spectroscopy; PSCs

1. Introduction

Semiconducting polymer photovoltaic cells which are fabricated by conjugated polymer donor such as poly(3-hexylthiophene-2/5-diyl)(P3HT) and fullerene derivative acceptor materials such as [6,6]-phenyl-C61-butyric-acid-methyl-ester(PCBM) have attracted great attention owing to their simple device structure, easy fabrication, less weight, weight together with optically and electronically adjustable molecular structure [1,2]. Due to high charge carrier mobility as well as

thermal stability [3,4], PCE of P3HT/PCBM PSCs reached to 5% as reported by Ma et al. [5]. However with structural and morphological improvements, PCE of polymer solar cells reached up to more than 9% [6,7]. Recently, Jung et al. [8] has reported 18% PCE for nanostructure based organic photovoltaic devices.

Organic semiconducting materials in the active layer create bounded electron-hole pairs with small diffusional lengths after absorbing photons from light rather than creating free carriers with longer diffusional lengths. Therefore, P3HT/PCBM layer thickness is limited to a few hundred nanometers in order to discourage the recombination of charges. This photoactive films also lead to optical transmission loss of incident light [9,10]. The traveling-length of the incident photons in the absorber material should be reduced without changing the absorber thickness to minimize the optical transmission loss in the polymer thin film [11,12]. Several strategies have been implemented by several researchers to improve the photon absorption ability in thin film including utilizing the light trapping method associated with excited plasmonic particles. The localized surface plasmon resonance (LSPR) can occur in illuminated metallic nanoparticles, like gold nanoparticles (Au-NPs), when oscillations of the incident electric field resonate with the surface electronic charges on those nanoparticles. This resonance effect allows Au-NPs to absorb light in the visible region of the spectrum leading to intensification by a factor of 100 in the electromagnetic (EM) field surrounding them [13]. Therefore, Au-NPs are popular in thin film solar cells since they enhance the light absorption by employing far-field or near-field effects associated with the localized surface plasmon resonance (LSPR) in the thin film [14–16].

Tremendous research work has been carried out on tuning the polymer solar cells with Au-NPs. Chen et al. [17] reported 4.19% PCE with a 20% improvement in gold NPs (35 nm) incorporated hybrid photovoltaic devices. Xie et al. [18] incorporated relatively small Au-NPs (18 and 35 nm in diameter) into Poly (3,4-ethylenedioxythiophene)-poly(styrenesulfonate) (PEDOT/PSS), P3HT/PCBM films, achieving 2.15% maximum PCE with 22% enhancement. This improvement was attributed to better hole collection at anode with the addition of Au-NPs to the PEDOT:PSS layer. The addition of Au-NPs to P3HT/PCBM active layer also contributes to enhanced optical absorption, thus introducing a more balanced charge-transport phenomenon. Wang et al. [19] reported that incorporation of Au-NPs (∼70 nm) into active layers of the PSCs leads to a significant enhancement in short circuit current density (J_{sc}), fill factor (FF), and PCE. This enhancement was attributed to enhanced photo absorption by the light scattering of Au-NPs in the active layer. The incorporation of Au-NPs both in PEDOT/PSS and active film resulted in ∼22% increase of PCE [20]. However, incorporation of Au-NPs only in PEDOT/PSS [21] improved the PCE from 6.4%–7.6% with 18% enhancement due to the forward-scattering of NPs. Chen et al. [22] reported a strong near field surrounding gold NPs caused by LSPR which is distributed horizontally through PEDOT/PSS, resulting in marginal photon absorption increment of P3HT/ PC70BM film. Choy et al. [23] reported that the plasmonic resonance in the semiconductor-metal interface can enhance the light absorption and photoexcited carrier generation occurring in PSCs. In addition, metal nanoparticles improve both hole-electron mobility and charge carrier transport in the active layer. The incorporation of small Au NPs into the active layer improved the short-circuit current (Jsc) from 4.16 mA cm^2 to 4.67 mA cm^2. Consequently, the addition of large Au NPs increased the Jsc from 10.3 mA cm^2 to 11.18 mA cm^2 with 3.54% to 4.36% enhancement in PCE [24]. Gan et al. [25] reported that the incorporation of Au NPs (15 nm in diameter) in the PEDOT: PSS layer with poly(2-methoxy-5(20-ethylhexyloxy)-1,4-phenylenevinylene (MEH-PPV) active layer enhanced the PCE from 1.99% to 2.36% with 19%

improvement. Randomly distributed Au nanowires which were embedded at the interface between PEDOT:PSS and ITO layers improved the PCE from 2.31% to 2.45% with enhanced plasmon excitation and far-field scattering.

In a related work reported elsewhere by our research group, copper oxide nanoparticles (CuO NPs) were successfully incorporated into the P3HT/ PC70BM ([6,6]-phenyl-C71-butyric-acid-methyl-ester) active layer. The PCE of the PSCs increased by 40.9% to 2.96% in cells with 0.6 mg of CuO-NPs due to enhanced carrier generation ability of P3HT/PCBM thin film [26]. However, no conclusive work has been conducted to optimize the PCE of PSCs using both CuO NPs and Au NPs incorporated in the active layer and hole transport layer respectively. This research work shows the increment of PCE and J_{sc} of P3HT/PC70BM bulk heterojunction solar cells by addition of gold (Au) and copper oxide (CuO) NPs in the PEDOT:PSS and active layer respectively. The combine effect of Au NPs in the PEDOT:PSS and CuO NPs in the P3HT/PC70BM on the device efficiency were studied by External quantum efficiency (EQE), atomic force spectroscopy (AFM), UV absorption and their current density- voltage (J-V) characteristics.

2. Materials and Mehods

2.1. Materials

Under the same experimental conditions, a set of polymer based photovoltaic devices which were varying in their Au and CuO NPs content were fabricated and tested. P3HT was bought from Rieke Metals and PC70BM from SES Research. They were used as received. PEDOT/PSS mixed in distilled water was obtained from Sigma Aldrich and same amount of distilled water was added. Online purchasing (Nanocs, Inc) was done for conducting glass substrates (24 × 80 × 1.2 mm (12 Ω/cm^2) and conducting layer 25 to 100 nm). Au (18 nm diameter) and CuO (100 to 150 nm diameter) NPs also were ordered online (nanocs.com). Airgas-company supplied purified N_2 gas and Al coils with a diameter of 0.15 mm were obtained online (Ted-Pella).

2.2. Solar cell fabrication

The fabrication of Polymer based solar cells containing gold and copper oxide NPs was done in a glove box using N_2 as the inert atmosphere. The P3HT:PCBM:CuO NPs blends were obtained in two-steps. First, the P3HT-PC70BM blend was obtained by diluting same amount of regioregular P3HT and PC70BM (10 mg each) with 2 ml of chlorobenzene (C_6H_5Cl) and mixed constantly for 14 hours at a temperature of 60 ^oC. CuO NPs also were dispersed in the same volume of C_6H_5Cl and added to the above mixture, so that weight ratios of ingredients (P3HT/PCBM/CuO-NPs) in the final blend was 10:10:0.6 mg. In addition, different amounts of Au NPs were added to 10 ml of PEDOT: PSS aqueous solution, leading to six PEDOT: PSS solutions with 0, 0.02, 0.06, 0.10, 0.14, and 0.18 mg of NPs; respectively.

The solar cell device structure that was spun coated in this research is schematically presented in figure 1. In a glove box with N_2 environment, the solar cell devices were spun coated by installing the PEDOT/PSS film on a conductive glass plate and P3HT/PC70BM film on the top of it. Using ultrasonic cleaning method, the conducting glass substrates were cleaned with ammonium hydroxide, hydrogen peroxide, distilled water, methyl alcohol, and isopropyl alcohol successively. The 40 nm-

thick PEDOT/PSS/Au layers, which serve as thin hole-transport layers, were prepared by spun-coating at rotational velocity of 4000 rpm followed by heating at 120 °C for 20 minutes in air. After the temperature of the samples came back to ambient temperature, the blends with P3HT:PC70BM: CuO NPs were spun coated at 1000 rpm for one to two minutes. This active layer had 120 nm average thicknesses and the device had 0.12 cm^2 surface area. Annealing was performed on all devices inside an inert oven for 30 minutes after Al electrode deposition. The annealing temperature was 150 °C.

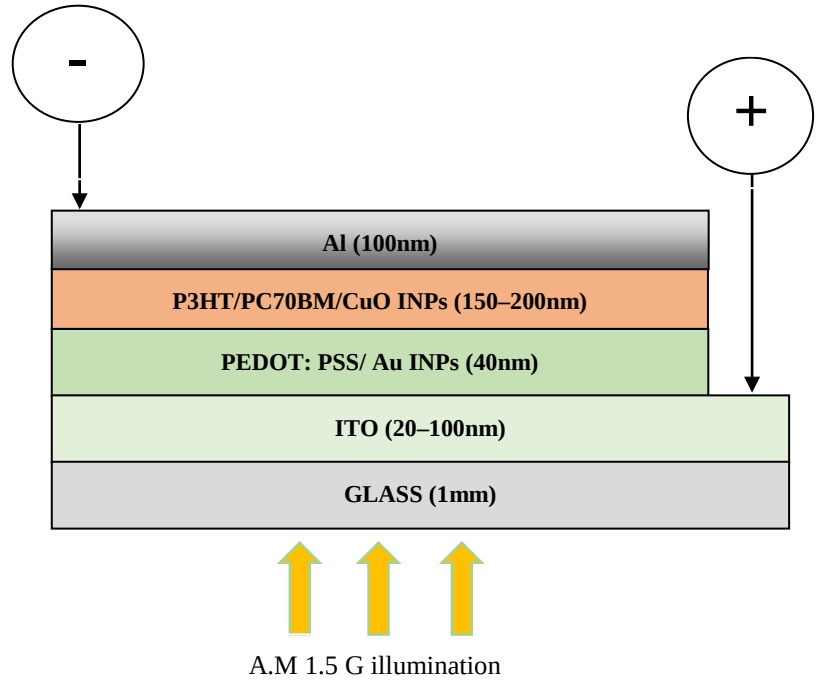

Figure 1. Graphical representation of the hybrid device architecture.

2.3. Solar cell characterization

Under the general laboratory environment, the electronic and thermal behaviour of PSCs with a constant CuO NP content and different amount of Au NPs were analysed. Current density-voltage (J-V) characterization was carried for all PSCs. UV solar simulator consists of AM 1.5G filter and lamp intensity of 100 mW/cm^2 was used. A source meter (Keithley 2400) was employed to obtain the J-V measurements. Device parameters such as short circuit current (J_{sc}), open circuit voltage (V_{oc}), FF and power conversion efficiency were recorded in the PSCs containing varying amounts of gold NPs under ambient environment.

A quantum efficiency measurement kit (Newport-425) embedded in the solar cell simulator was used to obtain EQE values. Using PerkinElmer LAMBDA 650 spectrophotometer, the optical properties of samples containing varying amounts of gold NPs were obtained. Agilent 5420 atomic force microscope was used to analyze the surface morphology. The Pico Image Basics and Gwyddion software were utilized to determine the root mean square roughness (σ_{rms}) of surface under ACAFM noncontact mode with set point 1.60, I-gain of 10 and scanned area of 2 × 2 μm.

3. Results and Discussion

3.1. Performance characteristics

The composition and structure of the fabricated cells is represented as: ITO/PEDOT:PSS (with various amount of Au-NPs)/P3HT/PCBM (with 0.6 mg CuO-NPs)/Al. The table 1shows the summarized photovoltaic parameters, such as J_{sc}, V_{oc}, fill factor (FF) (equation 1), and PCE (equation 2) [22], of all the fabricated devices.

$$FF = \frac{J_m V_m}{J_{sc} V_{oc}} \tag{1}$$

$$PCE = \eta = \frac{J_{sc} V_{oc}\, FF}{P_{in}} \tag{2}$$

Summarized data indicates that the V_{oc} remained nearly the same after adding Au-NPs into PEDOT:PSS layer. The J_{sc} shows an increment from 6.484 to 7.491 mA/cm^2. FF values enhanced from 68 to 69.21%. These improved J_{sc} and FF influenced on PCE and it was enhanced from 2.963 to 3.51%. The incorporation of Au-NPs in the PEDOT:PSS layer contributed to about 18% increase in PCE due to the notably enhanced J_{sc} and improved *FF*. With increasing concentrations of Au-NPs in PEDOT:PSS layer up to 0.06 mg, the PCE of the solar cells increased proportionally and then started to decline significantly beyond that point.

Table 1. Device parameters of ITO/PEDOT:PSS (with Au-NPs)/P3HT/PCBM/CuO-0.6 mg NPs/Al solar cells.

Au-NPs(mg)	J_{sc}(A/cm^2)	V_{oc}(V)	FF(%)	PCE(%)
0	6.484	0.673	68.00	2.963
0.02	7.006	0.678	68.52	3.255
0.06	7.491	0.677	69.21	3.510
0.10	6.901	0.685	67.02	3.168
0.14	5.984	0.671	67.54	2.712
0.18	4.195	0.673	65.91	1.861

The *J-V* characteristics of six PSC devices which contained different amounts of Au NPs in the PEDOT:PSS layer are shown in Figure 2. The performance of cells has improved with increasing Au-NPs in the PEDOT:PSS layer.

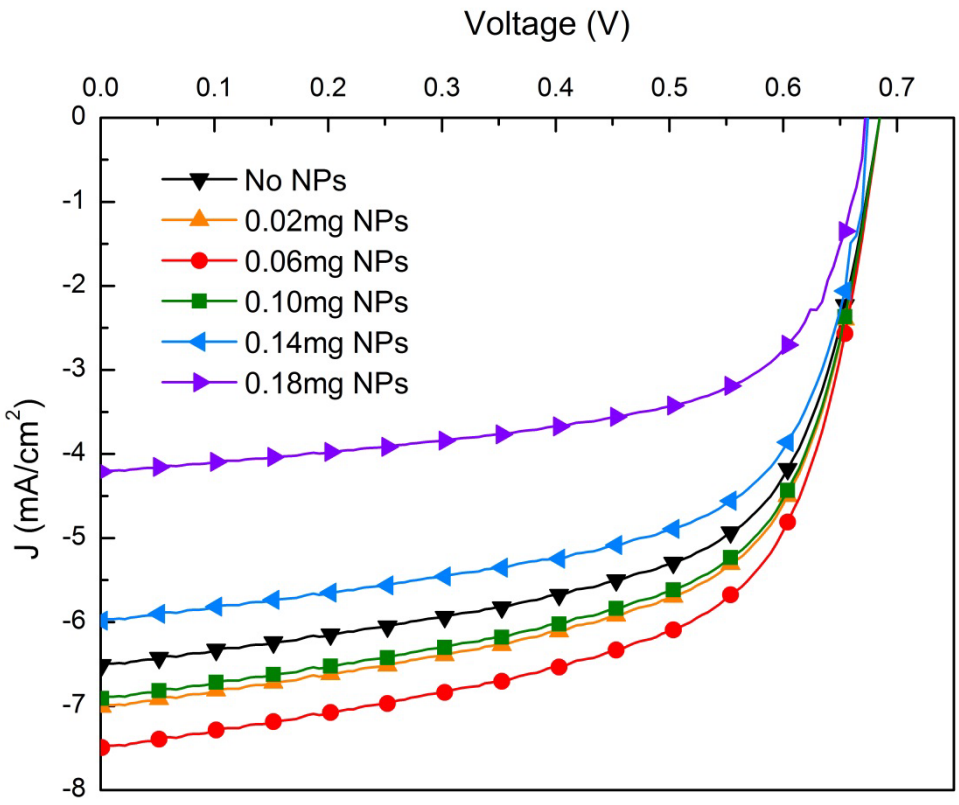

Figure 2. *J-V* characteristics of hybrid polymer solar cells with different amount of Au NPs in PEDOT: PSS layer

The J_{sc} has a linear relationship with the EQE of the solar cell devices. This relation is theoretically indicated as equation 3:

$$J_{sc} = \frac{q}{\hbar C} \int_{\lambda_{min}}^{\lambda_{max}} EQE\ P_{in}(\lambda)\ \lambda\ d\lambda \tag{3}$$

where q is the value of the charge, P_{in} is the input power, $\hbar$ is the reduced Planck constant, C and λ are the velocity and the wavelength of the light respectively [27].

The EQE measurers the ratio between the incident photons on the solar cell from the input source and the generated free charge carriers by the solar cell. EQE spectra of six different solar cells were first conducted to better elucidate improved J_{sc}. Corresponding EQE spectra for solar cells are presented in Figure 3. According to the equation 1, λ_{min} and λ_{max} represent the starting wavelength (300 nm) and the ending wavelength (800 nm) in the EQE spectrum.

The maximum EQE values were found to increase with the increasing amounts of Au-NPs in the PEDOT:PSS layer and then decreased as the amount of Au-NPs was increased beyond 0.06 mg. The J_{sc} values obtained for each cell followed a similar trend to EQE, which shows that the cells with 0.06 mg of Au NPs in the PEDOT:PSS layer exhibit the highest J_{sc} values. Figure 4 depicts the corresponding EQE and J_{sc} behaviour respectively.

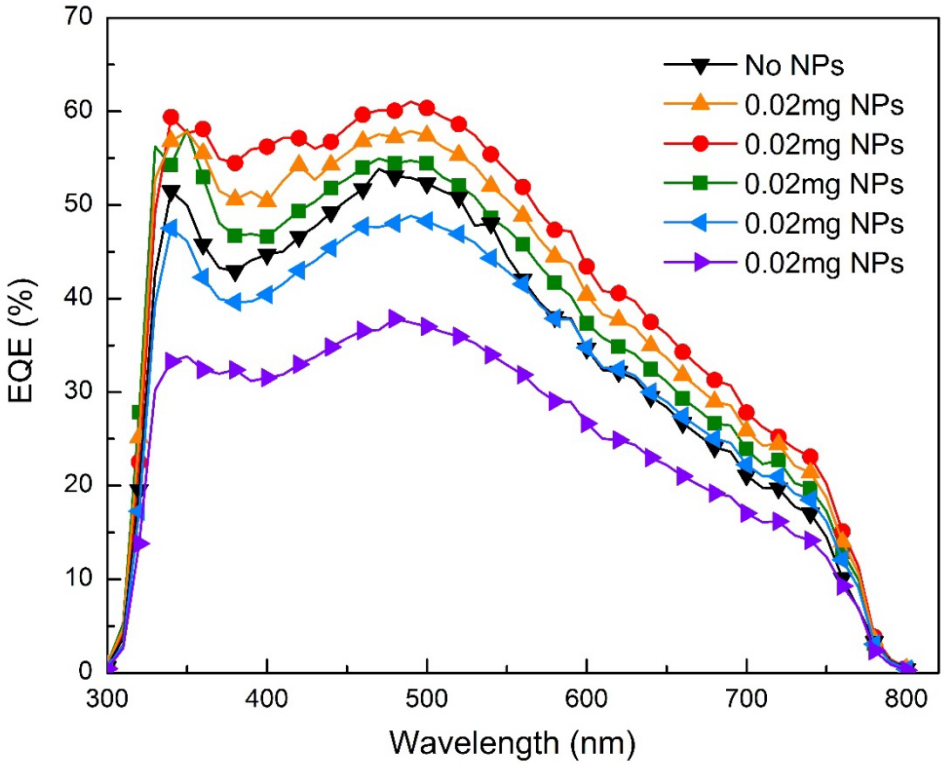

Figure 3. EQE of the hybrid solar cells with various Au NP concentrations in PEDOT: PSS.

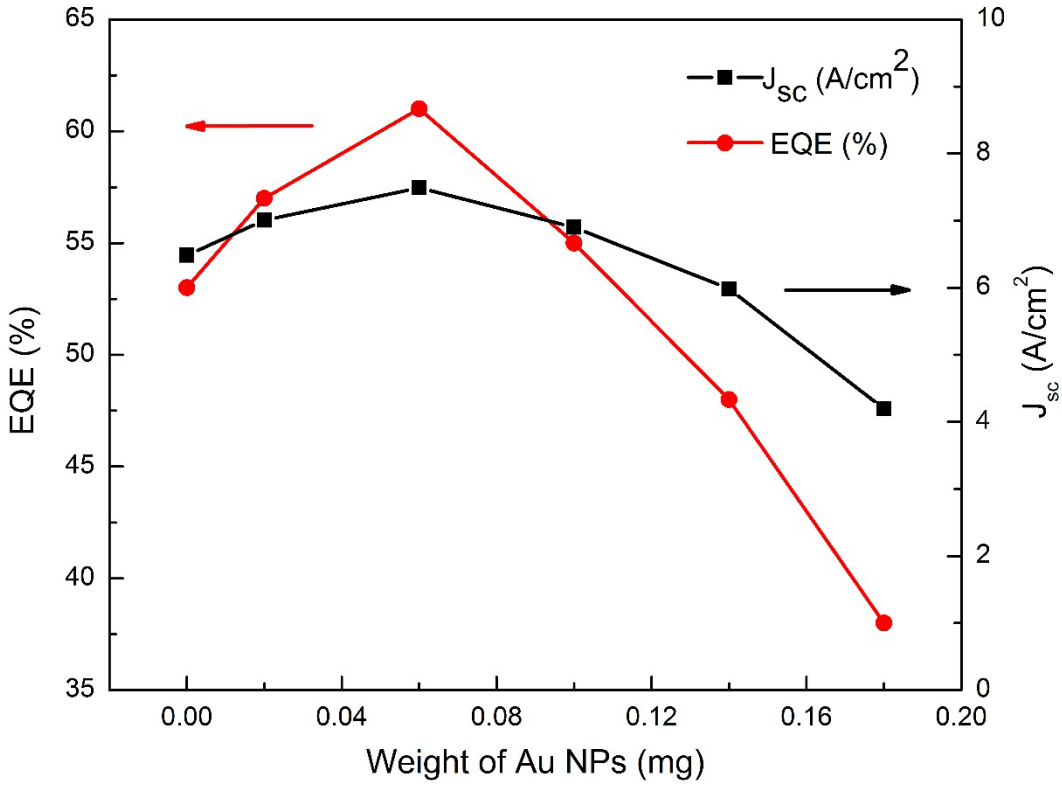

Figure 4. EQE and J_{sc} of the hybrid solar cells.

For successful photovoltaic operation, EQE can be determined by five major steps, these steps are composed with inherent efficiency components [26].

$$EQE = \eta_A . \eta_{diff} . \eta_{diss} . \eta_{tr} . \eta_{cc} \quad (4)$$

Here, η_A, η_{diff}, η_{diss}, η_{tr} and η_{cc} are represented the light absorption efficiency, the excitonic diffusion efficiency, the excitonic dissociation efficiency, the charge transport efficiency, and the electrons-holes collection efficiency respectively.

Generally, photo absorption and carrier generating ability of a polymer thin film are represented by the photon absorption (η_A) efficiency. The photo absorption of a semiconductor thin film is controlled by the energy band structure, light absorption coefficient and the photoactive layer thickness of the device. The surface morphology of the thin film also will affect the absorbance of the bulk heterojunction photoactive layer. Free charge carriers, which are produced by the light absorption, contribute effectively to enhance the J_{sc} of a hybrid device [28]. In hybrid solar cell fabrication, metal and inorganic nanoparticles can be used to enhance the photon absorption yield and improve the surface morphology of the thin films. This indicates that generated free electron composition of the metal and inorganic nanoparticles can influence the J_{sc} of the polymer based devices as well.

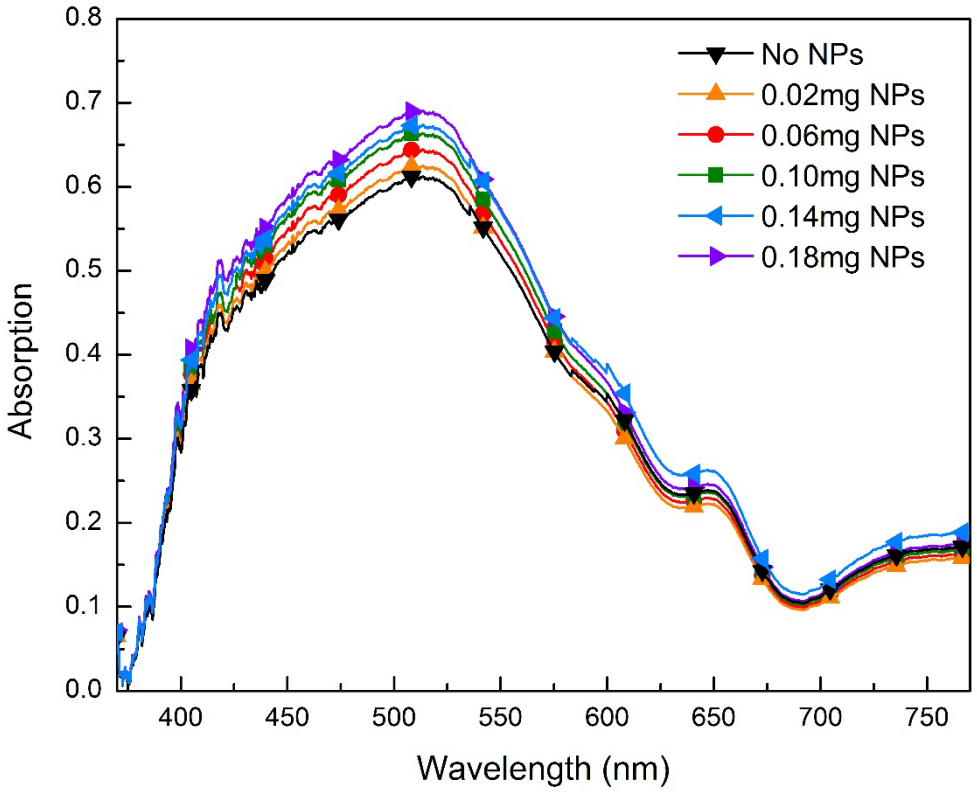

Figure 5. Optical absorption spectra of the hybrid solar cells with various Au NP concentrations in PEDOT: PSS layer.

To understand the J_{sc} enhancement, the UV-vis absorption measurements of the solar cells were obtained with and without Au-NPs in the PEDOT:PSS layer. The optical absorption spectra of Au nanoparticle incorporated PEDOT:PSS/ P3HT/PCBM/ CuO-NPs solar cells are shown in the figure 5.

3.2. Plasmonic effect of Au NPs in the PEDOT: PSS layer

The physics of plasmonic effect of Au-NPs doped into the PEDOT:PSS layer, which has been studied previously by Fung et al. [29], is in good agreement with our data. The absorption spectra of the PEDOT:PSS/P3HT/PCBM/CuO-NPs devices did not show any significant improvement increase of Au NPs concentration in the PEDOT:PSS thin film, as shown in Figure 5. This is caused by the strong near field surrounding the Au NPs due to the LSPR which is distributed horizontally through the PEDOT:PSS thin film, instead of penetrating upward into the P3HT/PC70BM layer, thus causing less optical absorption.

However, the EQE spectra of the PEDOT:PSS:Au NP devices increased significantly with the Au-NPs. Addition of 0.06 mg Au-NPs exhibit the highest EQE of 61% at a wavelength of 500 nm, as shown in Figure 3. At higher concentrations of Au-NPs, the EQE started to decrease. This is in good agreement with the trend of J_{sc}. It appears that; there is a discrepancy between light absorption and EQE spectrum. According to Equation (4), in addition to the light absorption, factors such as exciton dissociation rates and charge collection efficiencies also contribute to the magnitude of EQE. Therefore, it can be concluded that electrical effects, instead of plasmonic effects, play a major role in the solar cell performance. Since PEDOT:PSS layer (with or without Au NPs) did not significantly contributed to the photon absorption, the light absorption measurements only represent the inherent light harvesting within the active layer composed of P3HT/PC70BM/CuO-NPs. The absorption spectra in Figure 5, which show insignificant difference, indicates that the light absorption in P3HT/PCBM is unaffected by the incorporation of Au-NPs.

The AFM surface morphology of the PEDOT:PSS:Au-NP thin films with various concentrations of Au-NP, is shown in Figure 6. The AFM images showed a clear enhancement in surface roughness with increasing the Au-NP concentrations in PEDOT: PSS layers.

Table 2. The root-mean-square roughness values of the Au NPs added PEDOT: PSS layers.

Au-NPs(mg)	**The root-mean-square roughness σ_{rms}(nm)**
0	0.37
0.02	0.55
0.06	0.86
0.10	1.02
0.14	1.11
0.18	1.26

The σ_{rms} of the control layers was 0.37 nm and it was enhanced to 1.26 nm in the samples containing 0.18 mg of gold NPs. The cell with 0.06 mg of Au-NPs exhibited a surface roughness value of 0.86 nm as the best performed solar cell. (Table 2).

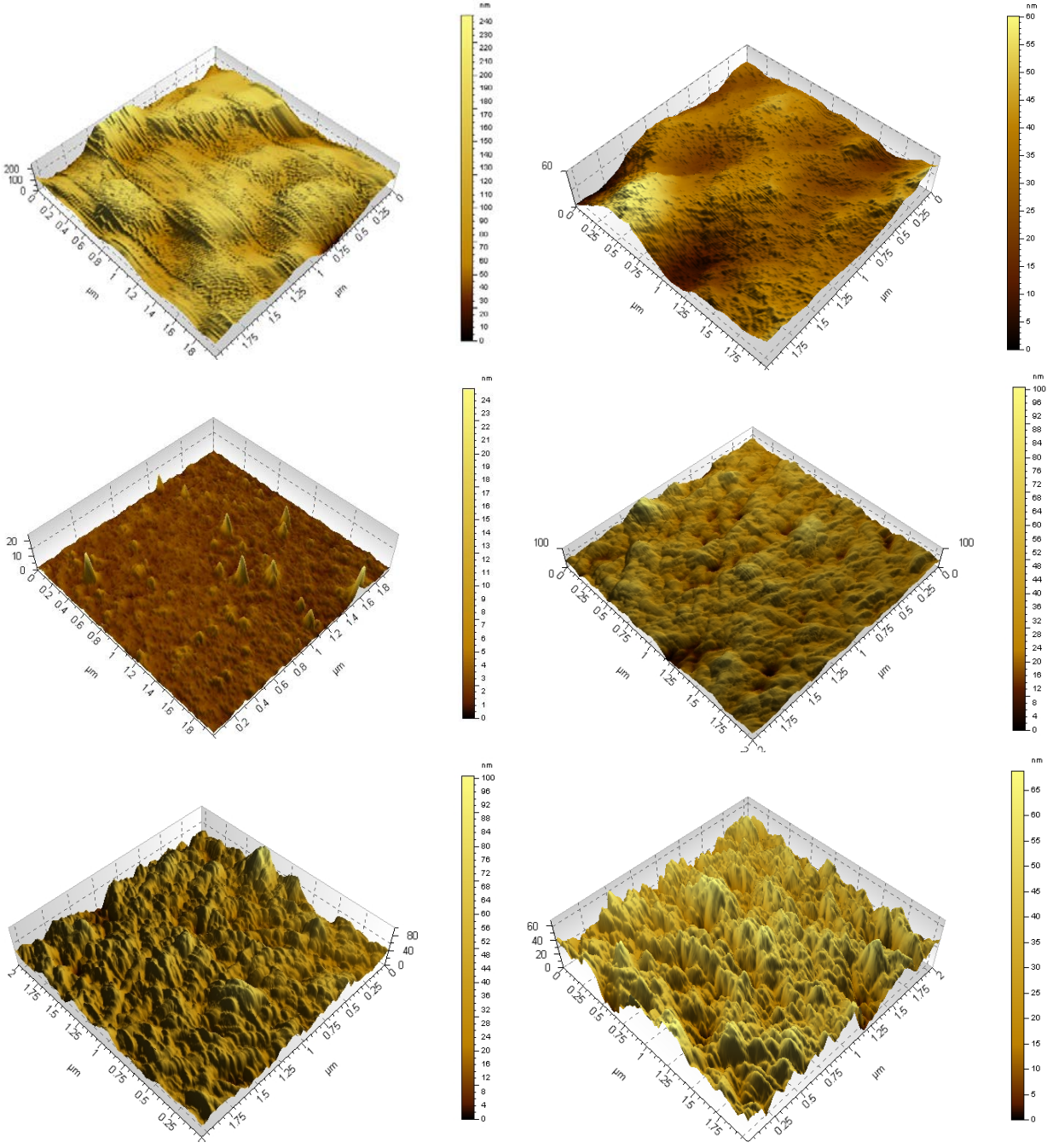

Figure 6. AFM images (non-contact mode) of PEDOT:PSS layers (2 × 2 μm scans) with (a) No Au NPs, (b) 0.02 mg Au NPs, (c) 0.06 mg Au NPs, (d) 0.10 mg Au NPs, (e) 0.14 mg Au NPs, (f) 0.18 mg Au NPs.

Hsu et al. [30] as well as Fung et al. [29] reported that a higher anode surface roughness leads to an increase in the interface contact area between the anode and the active layer in addition to shorter routes for holes to travel to the anode. This will cause to a higher efficiency of hole collection; thus

improving the J_{sc} of the devices. The holes collected at the anode can be independent from the external electric field by reducing the mean distance between the generated holes and the PEDOT:PSS which leads to higher fill factors (*FF*). Li et al. [31] suggested that the excitonic dissociation is encouraged by the defects sites, generated from rough P3HT/PCBM surface. The increased σ_{rms} of the PEDOT:PSS layer with presence of Au-NPs increases the contacting area between PEDOT:PSS and P3HT/PCBM. Hence, it improves the hole collecting ability at the roughened interface between PEDOT:PSS and P3HT/PCBM molecules leading to enhanced device performance. The electron and hole movability in polymer films is an important factor which depends on the charge carrier hopping rate and it should be high enough to avoid the carrier recombination.

It was suggested by Kim et al. [32] that the Au NPs introduce dopant states in molecular structure which can produce hopping sites for the holes resulting in a higher hole mobility. However, further increase of Au NPs, exceeding the optimum amount of 0.06 mg, allows the Au NPs to penetrate to P3HT/PCBM film and changing nanoscale morphology within P3HT/PCBM blend. This morphology change causes a significant reduction of donor/acceptor contact surface. The modified donor/acceptor contact surface proportionally affects the excitonic dissociation, thus lowering the EQE and J_{sc} of the cells [22,33].

3.3. Effect of CuO NPs in the active layer

The active layer of the device is composed of P3HT as the donor, PC70BM as the acceptor material and 0.6 mg of CuO-NPs. Even though the PEDOT:PSS layer did not exhibit absorption enhancement with or without Au-NPs, the P3HT/PC70BM active layer displayed a significant enhancement in absorption after incorporating CuO-NPs into the active layer [26]. The absorption spectrum of the reference cell, shown in Figure 5, is related to the absorption enhancement due to the CuO-NPs in the active layer. The P3HT molecules and CuO-NPs can generate excitons after absorbing the light photons with the energy than the E_g value (1.99 eV for P3HT and 2.07 eV for CuO-NPs) which reach to the P3HT/PC70BM and CuO-NPs/PC70BM interfaces respectively. Since there is no penetrated electric field to obstacle their motion through conjugated polymer, they diffuse by the force created with concentration gradient. This exciton diffusion to D/A interfaces is an essential phenomenon for exciton dissociation. The excitons which could not travel to D/A interface will not produce charge carriers (electrons or holes).

The PSCs with CuO NPs incorporated active layer can provide better routes for carrier transportation through inter-particle hopping sites in the structure which lead to an enhanced charge collection efficiency. It could be the possible reason behind the improved PCE of CuO-NPs incorporated PSCs. The optimum amount (0.6 mg) of CuO-NPs together with unbroken nanostructure creates an excellent interconnected network for the D/A nanoscale interlinking. Furthermore, the inter-nanoparticle hopping is encouraged by this system providing direct and efficient carrier transport routes for electrons and holes. Additionally, improved excitonic diffusion and carrier transport efficiencies imply that the life-time of the photo-generated carriers in detached state is enhanced, reducing the recombination probability. These factors will positively improve the *EQE* and *FF*, and thereby PCE.

The charge injecting possibility from the photo active layer to the electrodes is represented by the charge collection efficiency. The Au-NPs in the PEDOT:PSS also provide a better facility for

hole collection at the anode. The magnitude of the conduction band energy level of the accepter material is a critical parameter for better electron injection into the cathode. For possible electron injecting, this should be lower than the work function of donor [34]. Correspondingly, the magnitude of conduction band energy level should be greater than the work function of the anodic material for possible hole injection to anode. Figure 7 shows the energy level structure of the PEDOT:PSS/P3HT/CuO/PCBM device.

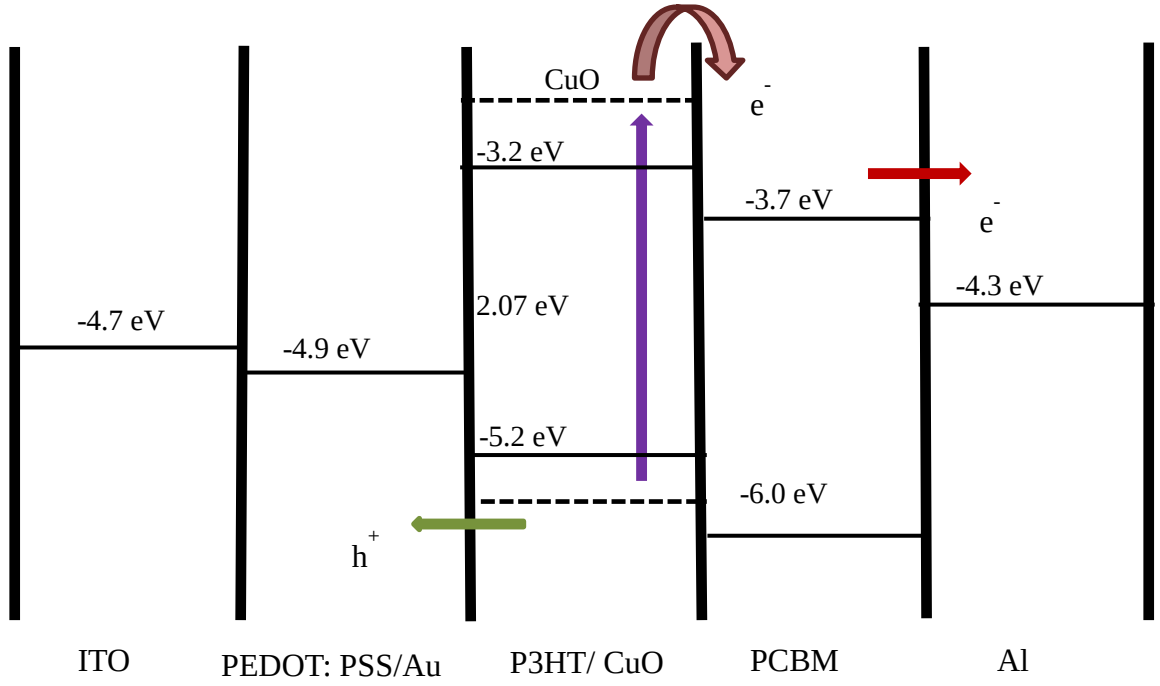

Figure 7. Energy band diagram of the P3HT/PCBM/CuO NP device [35].

As illustrated in the diagram, conduction and valence bands of P3HT and PC70BM are most suitable for donor and acceptor pair. The energy levels of the conduction and valence bands of CuO NPs are comparable with the lowest unoccupied molecular orbital (LUMO) and highest occupied molecular orbital (HOMO) of PC70BM acceptor. Therefore, CuO-NPs/PC70BM are a suitable donor and acceptor pair and a semiconductor heterojunction can be formed between them. The energy band structures of the PEDOT:PSS and Au-NPs are compatible with the energy levels of P3HT providing a better route for holes. The created electrons in the active layer could be transferred from the conduction bands of the CuO and P3HT to PC70BM. Similarly the separated holes can be diffused from the valence bands of the CuO and P3HT to the ITO through the Au-NPs and PEDOT:PSS. CuO is a p-type, direct transition band gap inorganic semiconductor providing a great photo absorption in the active layer. Hence, CuO-NPs can be used as an efficient electron injector in the active layer.

The Au and CuO-NPs incorporated nanostructures have excellent transport roots for free electrons and holes through different possible pathways: 1) the conventional interconnected PCBM molecules, 2) the incorporated Au and CuO NPs, 3) the partially crystalline PCBM/P3HT and PEDOT:PSS amorphous domains composed with CuO and Au-NPs respectively. These multiple routes increase the carrier mobility and thus significantly enhance the EQE and PCE.

3.4. SEM and EDX analysis

The SEM image of layer structure of the fabricated Au-NPs/PEDOT:PSS/ CuO NPs/P3HT: PCBM device is shown in the Figure 8(b). The Au-NPs (18 nm diameter) added PEDOT: PSS layer has approximately 40 nm thickness. To eliminate the charge recombination losses, thickness of the P3HT/PCBM active layer was maintained at 100–150 nm. The EDX mappings of copper atoms in the active layer and Au in the PEDOT:PSS layer of the optimum solar cell with 0.06 mg of Au-NPs are shown in Figure 8(a) and 8(c). This can be used to indicate the distribution of CuO and Au NPs in the active layer and PEDOT:PSS layer respectively. It clearly illustrates that both NPs in the PEDOT: PSS and active layers are uniformly distributed avoiding agglomeration.

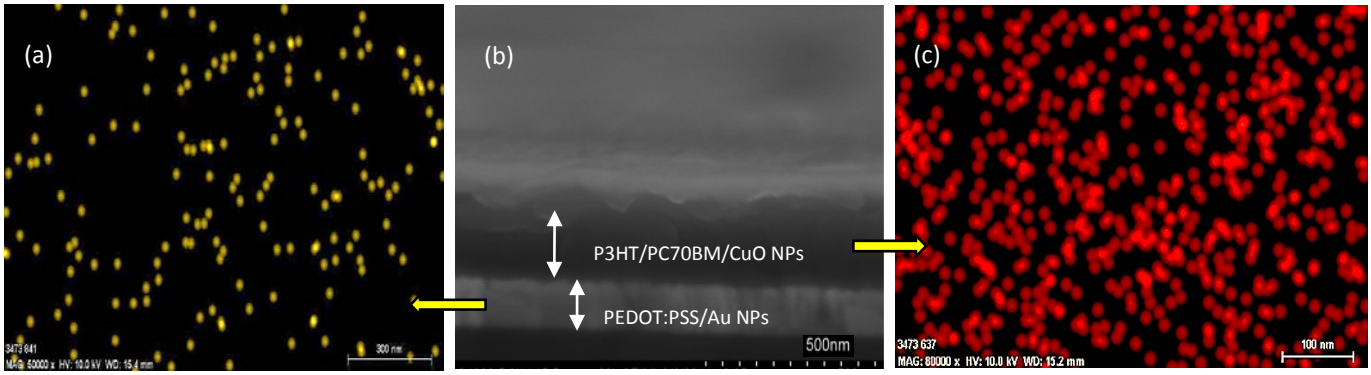

Figure 8. (a) EDX mapping showing the distribution of Au NPs in the PEDOT: PSS layer (b) SEM image of the hybrid polymer solar cell (c) EDX mapping showing the distribution of elemental copper in the P3HT/PCBM active layer.

Open circuit voltage (V_{oc}) has a linear relationship to energized band levels within D-A phases. The linear correlation of the V_{oc} to the energetic gap between donor's HOMO level and acceptor's LUMO level can be shown as equation 5 [35],

$$V_{oc} = E_{g,D/A} = E_{g,D} - (LUMO_D - LUMO_A) \quad (5)$$

The V_{oc} of a hybrid solar cell can be increased by moving the polymer HOMO level further away from the vacuum level [36]. However, V_{oc} did not change significantly, possibly since the LUMOs of P3HT and PC70BM were constant; thus suggesting that the reduced recombination due to increased carrier mobility did not improve V_{oc}. On the other hand, the HOMO energy level of P3HT in the active layer was not influenced by the Au-NPs in the PEDOT:PSS layer. Therefore; Au-NPs do not enhance V_{oc} in the solar cells, either.

4. Conclusion

In this study, Au-NPs were added at different amounts to the PEDOT:PSS layer of solar cells containing 0.6 mg of CuO-NPs in the P3HT/PC70BM layer in order to increase the power conversion efficiency. The PCE increased from 2.96% to 3.51% in the cells containing 0.06 mg Au-NPs, which is equivalent to 18.5% improvement in efficiency. The higher performance is attributed

to enhanced EQE, charge collection, exciton dissociation and interfacial distribution. The charge transport process was facilitated by providing better pathways in a continuous internal structure and hopping sites. The optical absorption spectrum did not change significantly in the presence of Au-NPs in the PEDOT:PSS layer due to the strong near field around Au-NPs. However, AFM analysis showed an increase in surface roughness of the PEDOT:PSS layer with Au-NPs, which indicates a larger contact area between PEDOT:PSS and the active layers. The photon absorption and charge harvesting increased remarkably due to the presence of CuO NPs in the active layer. EDX mappings revealed a uniform distribution of both Au and CuO NPs in the PEDOT:PSS and active layers; respectively.

Conflict of Interest

All authors declare no conflict of interest in this paper.

References

1. Abu-Zahra N, Algazzar M (2013) Effect of crystallinity on the performance of P3HT/PC70BM/n-dodecylthiol polymer solar cells. *J Sol Energy Eng* 136(2):021023.
2. Manceau M, Angmo D, Jorgensen M, et al. (2011) ITO-free flexible polymer solar cells: From small model devices to roll-to-roll processed large modules. *Org Electron* 12, 566–574.
3. Michael CH, Ali D (2014) Efficient generation of model bulk heterojunction morphologies for organic photovoltaic device modeling. *Appl Phys Rev* 2: 014008.
4. Choulis SA, Kim Y, Nelson J, et al. (2004) High ambipolar and balanced carrier mobility in regioregular poly (3-hexy thiophene). *Appl Phys Rev* 85: 3890–3892.
5. Ma W, Yang C, Gong X, et al. (2005) Thermally stable, efficient polymer solar cells with nanoscale control of the interpenetrating network morphology. *Adv Funct Mater* 15: 1617–1622.
6. Liao SH, Jhuo HJ, Yeh PN, et al. (2014) Single junction inverted polymer solar cell reaching power conversion efficiency 10.31% by employing dual-doped zinc oxide nano-film as cathode interlayer. *Sci Rep*, 4: 6813: 4–10.
7. Raja R, Liu WS, Hsiow CY, et al. (2015) Terthiophene-C60 dyads as donor/acceptor compatibilizers for developing highly stable P3HT/ PCBM bulk heterojunction solar cells. *J Mater Chem A* 3: 14401–14408.
8. Jung K, Song HJ, Lee G, et al. (2014) Plasmonic organic solar cells employing nanobump assembly via aerosol-derived nanoparticles. *ACS Nano* 8: 2590-2601.
9. Deibel C, Dyakonov V (2010) Polymer–fullerene bulk heterojunction solar cells. *Rep Prog Phys* 3: 9.
10. Gunes S, Neugebauer H, Sariciftci NS (2007) Conjugated polymer-based organic solar cells. *Chem Rev* 107: 1324–1338.
11. Atwater HA, Polman A (2010) Plasmonics for improved photovoltaic devices. *Nat Mater* 9: 205–213.
12. Schuller JA, Barnard ES, Cai W, et al. (2010) Plasmonics for extreme light concentration and manipulation. *Nat Mater* 9: 193–204.
13. Mahmoud AY, Izquierdo R, Truong VV (2014) Gold nanorods incorporated cathode for better performance of polymer solar cells. *J Nanomater* (2014): 464160.

14. Brown M, Suteewong T, Kumar R, et al. (2011) Plasmonic dye-sensitized solar cells using core-shell metal-insulator nanoparticles. *Nano Lett*: 11: 438–445.
15. Kim SS, Na SI, Jo J, et al. (2008) Plasmon enhanced performance of organic solar cells using electrodeposited Ag nanoparticles. *Appl Phys Lett* 93: 073307.
16. Chou SY, Ding W (2013) Ultrathin, high-efficiency, broad-band, omni-acceptance, organic solar cells enhanced by plasmonic cavity with subwavelength hole array. *Opt Express* 21: 60–76.
17. Chen FC, Wu JL, Lee CL, et al. (2009) Plasmonic-enhanced polymer photovoltaic devices incorporating solution- processable metal nanoparticles. *Appl Phys Lett* 95: 013305.
18. Xie F, Choy W, Wang C, et al. (2011) Improving the efficiency of polymer solar cells by incorporating gold nanoparticles into all polymer layers. *Appl Phys Lett* 99: 153304.
19. Wang DH, Kim DY, Choi KW, et al. (2011) Enhancement of Donor–Acceptor Polymer Bulk Heterojunction Solar Cell Power Conversion Efficiencies by Addition of Au Nanoparticles. *Angew Chem Int Ed* 50: 5519–5523.
20. Xie F, Choy W, Zhu X, et al. (2011) Improving polymer solar cell performances by manipulating the self-organization of polymer. *Appl Phys Lett* 98: 243302.
21. Baek SW, Noh J, Lee CH, et al. (2013) Plasmonic Forward Scattering Effect in Organic Solar Cells: A Powerful Optical Engineering Method. *Nat Sci Rep* 3: 1726.
22. Chen X, Zuo L, Fu W, et al. (2013) Insight into the efficiency enhancement of polymer solar cells by incorporating gold nanoparticles. *Sol Energy Mat Sol* 111: 1–8.
23. Choy W, Sha W, Li X, et al. (2014) Multi-Physical Properties of Plasmonic Organic Solar Cells. *Prog Electromag Res* 146: 25–46.
24. Choy W (2014) The emerging multiple metal nanostructures for enhancing the light trapping of thin film organic photovoltaic cells. *Chem Commun* 50: 11984–11993.
25. Gan Q, Bartoli FJ, Kafafi ZH (2013) Plasmonic-Enhanced Organic Photovoltaics: Breaking the 10% Efficiency Barrier. *Adv Mater* 25: 2385–2396.
26. Wanninayake AP, Gunashekar S, Li S, et al. (2015) CuO Nanoparticles Based Bulk Heterojunction Solar Cells: Investigations on Morphology and Performance. *J Sol Energy Eng* 137: 031016.
27. Wright M, Uddin A (2012) Organic-inorganic hybrid solar cells: A comparative review. *Sol Energ Mat Sol C* 107: 87–111.
28. Bundgaard E, Shaheen SE, Krebs FC, et al. (2007) Bulk heterojunctions based on a low band gap copolymer of thiophene and benzothiadiazole. *Sol Energ Mat Sol C* 91: 1631–1637.
29. Fung D, Qiao LF, Choy W, et al. (2011) Optical and electrical properties of efficiency enhanced polymer solar cells with Au nanoparticles in a PEDOT–PSS layer. *J Mater Chem* 21: 16349–16356.
30. Hsu MH, Yu P, Huang JH, et al. (2011) Balanced carrier transport in organic solar cells employing embedded indium-tinoxide nanoelectrodes. *Appl Phys Lett* 98: 073308-1.
31. Li G, Shrotriya V, Yao Y, et al. (2005) Investigation of annealing effects and film thickness dependence of polymer solar cells based on poly„3-hexylthiophen. *J Appl Phys* 98: 043704.
32. Kim K, Carroll DL (2005) Roles of Au and Ag nanoparticles in efficiency enhancement of poly(3-octylthiophene)/C60 bulk heterojunction photovoltaic devices. *Appl Phys Lett* 87: 203113.
33. Krebs FC, Thomann Y, Thomann R, et al. (2008) A simple nanostructured polymer/ZnO hybrid solar cell-preparation and operation in air. *Nanotechnology* 19: 424013.

34. Wanninayake A, Gunashekar S, Li S, et al. (2015) Performance enhancement of polymer solar cells using copper oxide nanoparticles. *Semicond Sci Technol* 30: 064004.
35. Nguyen BP, Kim T, Park CR (2014) Nanocomposite-based bulk heterojunction hybrid solar cells. *J Nanomater* (2014): 243041.
36. Eisenhawer B, Sensfuss S, Sivakov V, et al. (2011) Increasing the efficiency of polymer solar cells by silicon nanowires. *Nanotechnology* 22: 315401.

AIMS Press